A Robust Multi-Constraint Funnel MRAC System with Applications to Autonomous Multi-Rotor UAVs Transporting Payloads Connected by Ropes

Mattia Gramuglia*, Andrea L'Afflitto†
Virginia Tech, Blacksburg, VA, 24061

This paper presents a robust model reference adaptive control (MRAC) system that enforces hard constraints on the trajectory tracking error and soft constraints on the control effort at all times. A novelty of the proposed MRAC system lies in the fact that, if needed, user-defined constraints are adapted to be compatible with the controlled plant dynamics. Applied to the design of the outer loop of an autonomous X8 uncrewed aerial vehicle (UAV) transporting an unknown payload connected by a flexible rope, the proposed MRAC system provides improved solutions over similar state-of-the-art controllers.

I. Introduction

This paper proposes a robust model reference adaptive control (MRAC) system that enforces user-defined constraints. The constraints considered in this paper are of two kinds: hard constraints on a weighted norm of the trajectory tracking error and soft constraints on the control effort. This MRAC system allows enforcing time-varying constraints, and this explicit dependence on time is employed to regulate the diameter of the constraint set according to user-defined criteria, such as tightening the constraints on the tracking error if the actuators are far from saturating and loosening these constraints if the actuators are close to saturation. Within user-defined bounds, the diameter of the constraint set can be expanded to account for the effect of external disturbances, and subsequently reduced if more favorable conditions arise. This feature reduces the aggressiveness of the proposed control system over alternative ones.

The problem of enforcing user-defined, time-invariant hard constraints in MRAC systems has been investigated in numerous recent works, such as [1–3] to name some. The problem of imposing time-varying constraints on the tracking error has been studied in [4] and, more recently, in [5]. In [4], the authors designed an adaptive control system for linear time-invariant plant models in which the diameter of the constraint set is a decreasing function of time. The proposed results apply to nonlinear time-varying plant models. In [5], the diameter of the constraint set is an explicit function of time and of the tracking error and, hence, similarly to the controllers considered in this paper, can be set to account for the available control authority. Key differences between the proposed results and those in [5] are noteworthy. Firstly, [5] assumes that all nonlinear terms affecting the plant model are matched and captured by a regressor vector. Such a hypothesis is idealistic since, in practice, finite-dimensional representations of uncertainties, such as those provided by regressor vectors, never capture nonlinear effects completely [6, Ch. 1]. Furthermore, the use of a single regressor vector to capture the plant's nonlinear dynamics throughout the entire state space may be a strong assumption for problems of practical interest. Finally, if not all nonlinear terms are captured by a regressor vector and the adaptive control system is designed without accounting for unmatched uncertainties, then the adaptive gains may suffer from *parameter drift*, that is, the tracking error converges to zero at the expense of diverging adaptive gains. In this paper, we include unmatched uncertainties in the plant model and design a robust MRAC system that ensures boundedness and uniform ultimate boundedness of the closed-loop trajectory tracking error, as well as boundedness of the adaptive gains at all times. An additional remarkable difference between the proposed results and those in [5] lies in the rate of convergence of the diameter of the constraint set on the tracking error. In [5], either the constraint set contracts at the user-defined rate or, if such a rate of contraction is not compatible with the closed-loop plant dynamics, then the constraint set remains constant until more favorable conditions newly arise. This mechanism prevents the user from setting constraints that are incompatible with the plant dynamics. In the proposed control system, if the user-defined constraints contract too fast for the plant dynamics, then the diameter of the constraint set is contracted at a slower rate, but this process is not halted if the system's actuators have sufficient bandwidth to enforce tighter constraints on the tracking error.

*Graduate Student, Department of Mechanical Engineering.
†Associate Professor, Grado Department of Industrial and Systems Engineering, AIAA Associate Fellow.

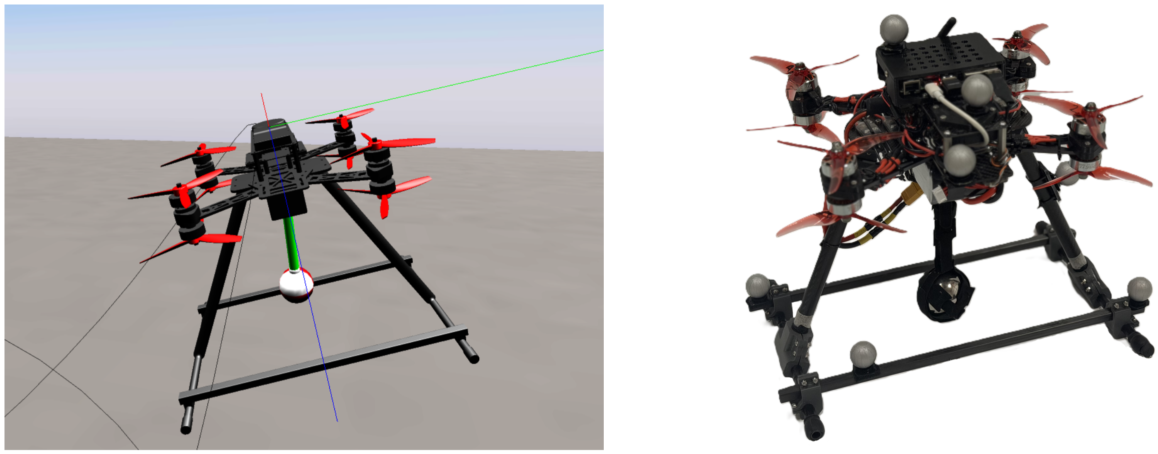

Fig. 1 Left: PyChrono-based simulation environment showing the X8-copter and suspended payload model used for the proposed numerical results. Right: X8-copter and payload configuration imported into the simulation environment. The geometry and inertial properties of the simulated UAV are derived from a detailed CAD (computer-aided design) model of the actual vehicle

The proposed results are tested in a simulation environment based on the high-fidelity physics engine PyChrono [7, 8]. In the proposed simulations, we consider an autonomous X8-copter uncrewed aerial vehicle (UAV) tasked with transporting a payload, which consists of a heavy steel ball connected to the UAV by a flexible rope. The simulator employed to perform the proposed numerical simulations is available at the GitHub repository [9]. Figure 1 shows an image captured in the simulation environment and the actual UAV, whose dynamics are simulated. A direct comparison with a robust MRAC system that is not designed to enforce user-defined constraints on the tracking error, and which is a special case of the proposed control system, clearly demonstrates the effectiveness of the proposed MRAC system in achieving smaller tracking errors with comparable control efforts.

In the proposed numerical simulations, the UAV is unaware of its payload; that is, the two control systems are tuned without the steel ball and the rope. Furthermore, the tunable parameters that are shared by both control systems are identical for the fairness of comparison. The `FEA` (finite-element analysis) module of PyChrono is leveraged to capture the dynamics of the payload and its effect on the UAV throughout the mission. The recognized effectiveness of this physics engine ensures high-quality results.

The problem of controlling UAVs transporting slung loads has gained considerable attention in recent years due to its wide-ranging applications in logistics, emergency response, and agriculture. However, transporting unsteady payloads presents notable challenges because of the complex coupled dynamics of the suspended payload and the UAV. Research in this domain can generally be classified into three macro-areas: results aimed at allowing the UAV to follow some user-defined trajectory despite the payload [10–12]; results aimed at allowing the UAV to follow some user-defined trajectory while aiming for payload swing suppression [13–16]; and results aimed at allowing the payload to follow some user-defined trajectory [17–20]. This work falls into the first research area since the proposed simulations aim to enable satisfactory trajectory tracking despite the unknown payload dynamics. Remarkably, to the authors' knowledge, this is the first work not to require modeling of the payload. This result has been possible by leveraging the robust nature of the proposed control systems and the adaptive mechanism that regulates the diameter of the constraint set.

For existing works, modeling the interaction between the rope and the payload is critical. Several papers model the cumulative effect of ropes using a spherical pendulum, and, hence, assume that the ropes are always taut [12–18, 21–23], which limits the aggressiveness of maneuvers. In some cases, the effect of ropes is captured by hybrid models that alternate taut and slack states [10, 11]. Finally, some studies model ropes as concatenated mass-spring-damper systems [19, 24, 25]. These modeling approaches, however, suffer from several limitations. For instance, the moments exchanged between the payload and the UAV through the rope are usually neglected [13, 15, 17, 21–23]. Furthermore, several papers rely on information that is difficult or impossible to deduce in applications of practical interest such as the force exerted by the rope [19, 21, 24] or the payload state [10, 13, 17, 18, 20, 22, 23, 25].

Numerous strategies have been examined in the literature to control a UAV transporting a slung payload. Among such strategies, it is worthwhile recalling sliding mode control [13, 21], disturbance rejection control methods [17], cascaded control systems [14], and adaptive controllers [16, 23, 25]. These techniques usually require precise knowledge of parameters such as cable length, payload mass, tension, or the payload's state. In some cases, disturbance estimators are required [15, 22]. Adaptive control methods often handle uncertainties in specific parameters, such as the cable length and the payload mass. The proposed control system departs significantly from the sensor- and model-reliant methodologies employed so far in the literature. Instead of employing dedicated sensors or estimators to verify the underlying assumptions, we consider the slung payload as an unmodeled uncertainty in the UAV dynamics.

This paper is structured as follows. In Section II, we formulate a problem statement. Section III briefly recalls the notion of the continuous convex projection operator and how it can be employed to enforce user-defined convex constraints on the adaptive gains of an MRAC system. In Section IV, we present the key theoretical result of this work. Section V illustrates the results generated through numerical simulations. Finally, Section VI summarizes the proposed results and outlines future work directions.

II. Problem Statement

Consider the plant model

$$\dot{x}(t) = Ax(t) + B\Lambda\left[u(t) + \Theta^{\mathrm{T}}\Phi(t, x(t))\right] + \xi_{\mathrm{d}}(t), \quad x(t_0) = x_0, \quad t \geq t_0, \tag{1}$$

where $x : [t_0, \infty) \to \mathbb{R}^n$ denotes the *plant state*, $u : [t_0, \infty) \to \mathbb{R}^m$ denotes the *control input*, $\Phi : [t_0, \infty) \times \mathbb{R}^n \to \mathbb{R}^N$ denotes the *regressor vector*, $A \in \mathbb{R}^{n\times n}$ is unknown, $B \in \mathbb{R}^{n\times m}$ is known and such that the pair $(A, B\Lambda)$ is controllable, $\Lambda \in \mathbb{R}^{m\times m}$ is diagonal, positive-definite, and unknown, $\Theta \in \mathbb{R}^{N\times m}$ is unknown and such that $\Theta^{\mathrm{T}}\Phi(t, x)$ captures matched uncertainties for all $(t, x) \in [t_0, \infty) \times \mathbb{R}^n$, and $\xi_{\mathrm{d}} : [t_0, \infty) \to \mathbb{R}^n$ is continuous, such that $\|\xi_{\mathrm{d}}(t)\| < \overline{\xi}_{\mathrm{d}}$ for all $t \in [t_0, \infty)$, where $\overline{\xi}_{\mathrm{d}} \geq 0$ is known, and captures unmatched uncertainties, such as, for instance, external disturbances. In MRAC problems, the plant trajectory $x(\cdot)$ must follow the trajectory of the *reference model*

$$\dot{x}_{\mathrm{ref}}(t) = A_{\mathrm{ref}}x_{\mathrm{ref}}(t) + B_{\mathrm{ref}}r(t), \quad x_{\mathrm{ref}}(t_0) = x_{\mathrm{ref},0}, \quad t \geq t_0, \tag{2}$$

where $x_{\mathrm{ref}} : [t_0, \infty) \to \mathbb{R}^n$ denotes the *reference trajectory*, $r : [t_0, \infty) \to \mathbb{R}^m$ is user-defined, continuous, uniformly bounded, and denotes the *reference command input*, $A_{\mathrm{ref}} \in \mathbb{R}^{n\times n}$ is user-defined Hurwitz, $B_{\mathrm{ref}} \in \mathbb{R}^{n\times m}$ is user-defined, and such that the pair $(A_{\mathrm{ref}}, B_{\mathrm{ref}})$ is controllable, and the matching conditions

$$A_{\mathrm{ref}} = A + B\Lambda K_x^{\mathrm{T}}, \tag{3a}$$

$$B_{\mathrm{ref}} = B\Lambda K_r^{\mathrm{T}} \tag{3b}$$

are verified by some $K_x \in \mathbb{R}^{n\times n}$ and $K_r \in \mathbb{R}^{n\times m}$. In this paper, we pursue multiple design goals. Our primary objective is to develop a robust MRAC system that ensures the uniform ultimate boundedness of the *trajectory tracking error* $e(t) \triangleq x(t) - x_{\mathrm{ref}}(t)$, $t \geq t_0$, despite uncertainties. Our second goal is to ensure that the tracking error remains within user-defined bounds that explicitly account for the actuators' bandwidth to adaptively tighten or loosen constraints on the tracking error as needed. For example, if the control effort is low, then the constraints on the tracking error are tightened. Alternatively, as the control approaches a user-defined value, the constraints on the tracking error are loosened. Our final goal is to utilize the continuous convex projection operator and impose user-defined constraints on the adaptive gains and, hence, prevent parameter drift.

III. Preliminaries on the Continuous Convex Projection Operator

To impose user-defined bounds on the adaptive gains and prevent parameter drift, in this paper, we employ a classical tool in MRAC theory, namely the continuous convex projection operator [26]. Given the relevance of this tool, it is worthwhile recalling its definition and key properties.

Definition III.1 *Let $\mathcal{D} \subseteq \mathbb{R}^n$ be convex, and let $h : \mathcal{D} \to \mathbb{R}$ denote a continuously differentiable convex function over $\mathcal{D}$ such that* $\inf_{x\in\mathcal{D}} h(x) < 0$. *The projection operator induced by $h(\cdot)$ over $\mathcal{D}$ is defined as* $\mathrm{proj} : \mathcal{D} \times \mathbb{R}^n \to \mathbb{R}^n$ *such* *that*

$$\operatorname{proj}(x, x_{\mathrm{d}}) \triangleq \begin{cases} x_{\mathrm{d}} - h(x) \dfrac{\left(\frac{\partial h(x)}{\partial x}\right)^{\mathrm{T}} \frac{\partial h(x)}{\partial x}}{\frac{\partial h(x)}{\partial x} \left(\frac{\partial h(x)}{\partial x}\right)^{\mathrm{T}}} x_{\mathrm{d}}, & \\ \qquad\qquad\qquad\qquad\qquad (x, x_{\mathrm{d}}) \in \mathcal{S}, & \\ x_{\mathrm{d}}, \quad \textit{otherwise}. & \end{cases} \tag{4}$$

where $\mathcal{S} \triangleq \left\{(x, x_{\mathrm{d}}) \in \mathcal{D} \times \mathbb{R}^n : h(x) > 0, \frac{\partial h(x)}{\partial x} x_{\mathrm{d}} > 0\right\}$.

A key property of the projection operator is that it allows constraining solutions of ordinary differential equations, such as adaptive laws, within user-defined convex sets. For the formal statement of this result, let $\mathcal{D} \subseteq \mathbb{R}^n$ be convex, let $h : \mathcal{D} \to \mathbb{R}$ denote a continuously differentiable convex function over $\mathcal{D}$ such that $\inf_{x \in \mathcal{D}} h(x) < 0$, and let

$$\overline{\Omega}_\alpha \triangleq \{x \in \mathcal{D} : h(x) \leq \alpha\}, \quad \alpha \in (-\inf_{x \in \mathcal{D}} h(x), 1]. \tag{5}$$

Theorem III.1 *Let $\mathcal{D} \subset \mathbb{R}^n$ be convex, let $h : \mathcal{D} \to \mathbb{R}$ denote a continuously differentiable convex function over $\mathcal{D}$ such that $\max_{x \in \mathcal{D}} h(x) = 1$ and $\inf_{x \in \mathcal{D}} h(x) < 0$, and let $x_{\mathrm{d}} : [t_0, \infty) \to \mathbb{R}^n$ be continuous. If $x_0 \in \overline{\Omega}_1$, then the solution of*

$$\dot{x}(t) = \operatorname{proj}(x(t), x_{\mathrm{d}}(t)), \quad x(t_0) = x_0, \quad t \geq t_0, \tag{6}$$

exists, is unique, and such that $x(t) \in \overline{\Omega}_1$, $t \geq t_0$.

The proof of this result, which can be found in [27, Ch. 11], shows that the projection operator gradually removes the component of $x_{\mathrm{d}}(\cdot)$ orthogonal to $\partial\Omega_1 \triangleq \{x \in \mathcal{D} : h(x) = 1\}$ and, if $x(t) \in \partial\Omega_1$ for some $t \geq t_0$, then the component of $x_{\mathrm{d}}(\cdot)$ orthogonal to $\partial\Omega_1$ is removed, and only the component of $x_{\mathrm{d}}(t)$ tangential to $\partial\Omega_1$ is retained.

The notion of projector operator can be extended from vectors to matrices as follows.

Definition III.2 *Let $\mathcal{D}_j \subseteq \mathbb{R}^{n+m+N}$ be convex, $j = 1, \ldots, m$, and let $h_j : \mathcal{D} \to \mathbb{R}$ denote a continuous differentiable convex function over $\mathcal{D}_j$ such that $\inf_{\pi \in \mathcal{D}_j} h_j(\pi) < 0$. The matrix convex projection operator induced by $h_j(\cdot)$, $j = 1, \ldots, m$, over $\prod_{j=1}^m \mathcal{D}_j$ is defined as $\operatorname{Proj} : \left(\prod_{j=1}^m \mathcal{D}_j\right) \times \mathbb{R}^{(n+m+N)\times m} \to \mathbb{R}^{(n+m+N)\times m}$ such that*

$$\operatorname{Proj}(X, X_{\mathrm{d}}) = \left[\operatorname{proj}(x_1, x_{\mathrm{d},1}), \ldots, \operatorname{proj}(x_m, x_{\mathrm{d},m})\right], \quad (X, X_{\mathrm{d}}) \in \left(\prod_{j=1}^m \mathcal{D}_j\right) \times \mathbb{R}^{(n+m+N)\times m}, \tag{7}$$

where $X = [x_1, \ldots, x_m]$ and $X_{\mathrm{d}} = [x_{\mathrm{d},1}, \ldots, x_{\mathrm{d},m}]$.

IV. Robust Funnel MRAC

To meet the design goals on the trajectory tracking error, we propose the following approach based on time-varying barrier functions over the compact *constraint set*

$$\mathcal{E}_t \triangleq \{e \in \mathbb{R}^n : H(t, e) \geq 0\}, \quad t \geq t_0, \tag{8}$$

where

$$H(t, e) \triangleq \eta_{\max} - \eta^2(t) - e^{\mathrm{T}} M e, \quad (t, e) \in [t_0, \infty) \times \mathbb{R}^n, \tag{9}$$

$\eta_{\max} > 0$ is user-defined, $M \in \mathbb{R}^{n\times n}$ is symmetric, positive-definite, and verifies the *algebraic Lyapunov equation*

$$-Q_{\mathrm{M}} = A_{\mathrm{ref}}^{\mathrm{T}} M + M A_{\mathrm{ref}}, \tag{10}$$

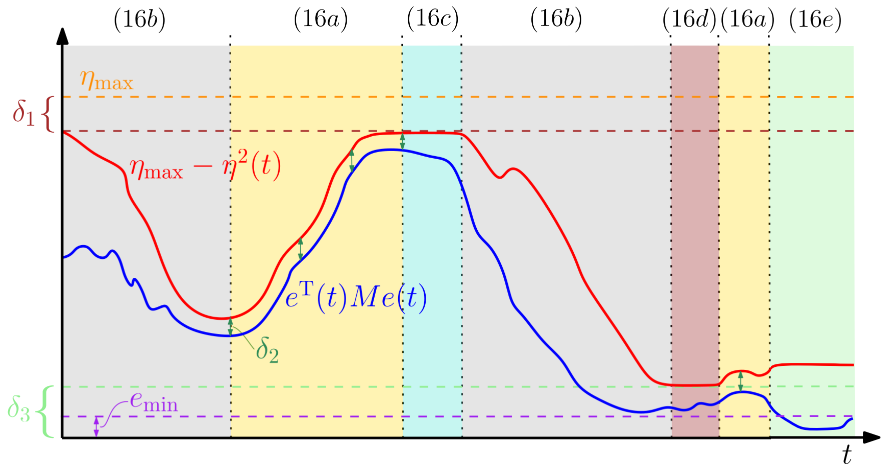

Fig. 2 Graphical representation of how the terms $\eta_{\max}$, $e_{\min}$ δ_1, δ_2, and δ_3 influence the funnel operational envelope. The tunable parameter δ_1 is introduced to ensure that $\eta(t) > 0$ for all $t \geq t_0$, and $\eta_{\max} - \delta_1$ represents the maximum funnel diameter. The tunable parameter δ_2 allows the user to impose a minimum distance between the funnel and the norm of the trajectory tracking error. The tunable parameter δ_3 is a lower bound on how much the funnel can contract. If the weighted norm of the tracking error is smaller than or equal to $e_{\min}$, the funnel adaptation mechanism is turned off

the matrix $Q_{\mathrm{M}} \in \mathbb{R}^{n\times n}$ is user-defined, symmetric, and nonnegative definite, $\eta : [t_0, \infty) \to \left[\sqrt{\delta_1}, \sqrt{\eta_{\max} - \delta_3}\right]$ is continuous, $\delta_3 > \delta_2 > 0$, $\delta_3 > e_{\min}$, $\eta_{\max} > \delta_1 + \delta_3 > 0$, and

$$e_{\min} \triangleq \frac{2\bar{\xi}_{\mathrm{d}}\lambda_{\max}(M)}{\lambda_{\min}(Q_{\mathrm{M}})}. \tag{11}$$

In this paper, we refer to the constraint set (8) as the *funnel* since, in nominal conditions, its diameter $\max_{e_1,e_2\in\mathcal{E}_t} \|e_1 - e_2\| = \eta_{\max} - \eta^2(t)$ is reduced as a user-defined function of time to enforce increasingly tighter constraints on the tracking error. As discussed below, in practice, $\eta(\cdot)$ is designed to maintain constant, increase, or decrease the diameter of the funnel to accommodate the user-defined constraints on both the tracking error and the control effort, as well as the effect of unmatched uncertainties.

Equation (10) is to be interpreted as a compatibility condition between the user-defined reference trajectory and the user-defined constraint set. The role of the user-defined function $\eta(\cdot)$ in (9), which regulates the diameter of the funnel, can be interpreted as follows. Let

$$\sigma_{\mathrm{nom}}(t) \triangleq \min\left\{\eta(t)\xi(t), \lambda_{\mathrm{sat}}(t, e(t))\right\}, \quad t \in [t_0, \infty), \tag{12}$$

where $\xi : [t_0, \infty) \to \mathbb{R}$ is continuous, uniformly bounded, and user-defined,

$$\lambda_{\mathrm{sat}}(t,e) \triangleq \frac{H(t,e)\left[\lambda_{\min}(Q) + V_e(t,e)\lambda_{\min}(Q_{\mathrm{M}}) - \nu - 2\bar{\xi}_{\mathrm{d}}/\|e\|\left(\lambda_{\max}(P) + V_e(t,e)\lambda_{\max}(M)\right)\right]}{2\lambda_{\max}(P)\eta(t)},$$
$$(t,e) \in [t_0,\infty)\times\mathbb{R}^n \setminus \overline{\mathcal{B}}_{e_{\min}}(0_n), \tag{13}$$

$\lambda_{\max}(\cdot)$ and $\lambda_{\min}(\cdot)$ denote the eigenvalues with largest and smallest real part of their arguments, respectively, the symmetric, positive-definite matrices $P, Q \in \mathbb{R}^{n\times n}$ verify the *algebraic Lyapunov equation*

$$-Q = A_{\mathrm{ref}}^{\mathrm{T}}P + PA_{\mathrm{ref}} \tag{14}$$

with Q user-defined, $\nu \in (0, \lambda_{\min}(Q))$ is user-defined,

$$V_e(t,e) \triangleq \frac{e^{\mathrm{T}}Pe}{H(t,e)}, \quad (t,e) \in \mathring{\mathcal{E}}_t, \tag{15}$$

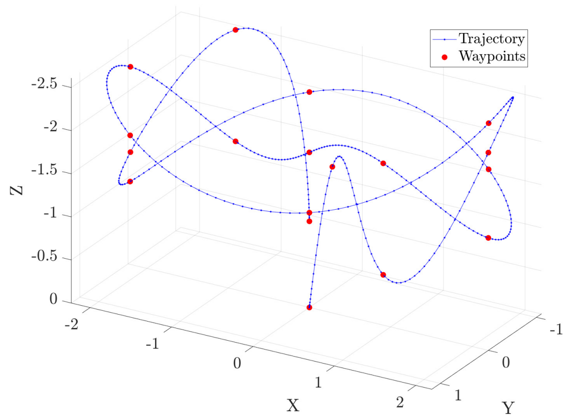

Fig. 3 Minimum-jerk user-defined trajectory to be tracked by the UAV. This trajectory interpolates 18 user-defined waypoints of a three-dimensional lemniscate

$\mathring{\mathcal{E}}_t \triangleq \{e \in \mathbb{R}^n : H(t, e) > 0\}$ denotes the *interior of* $\mathcal{E}_t$, and $\overline{\mathcal{B}}_\rho(0_n) \subset \mathbb{R}^n$ denotes the closed ball of radius $\rho > 0$ centered at the origin. The continuous function $\eta(\cdot)$ verifies one of these alternative laws

$$\dot{\eta}(t) = \min\left\{0, -\frac{e^{\mathrm{T}}(t)M\dot{e}(t)}{\eta(t)}\right\}, \quad \text{if } \|e(t)\| > e_{\min} \text{ and } H(t,e) = \delta_2 \text{ and } \eta(t) \in \left(\sqrt{\delta_1}, \sqrt{\eta_{\max} - \delta_3}\right), \tag{16a}$$

$$\dot{\eta}(t) = \sigma_{\mathrm{nom}}(t), \quad \text{if } \|e(t)\| > e_{\min} \text{ and } H(t,e) > \delta_2 \text{ and } \eta(t) \in \left(\sqrt{\delta_1}, \sqrt{\eta_{\max} - \delta_3}\right), \tag{16b}$$

$$\dot{\eta}(t) = \max\{0, \sigma_{\mathrm{nom}}(t)\}, \quad \text{if } \|e(t)\| > e_{\min} \text{ and } \eta(t) = \sqrt{\delta_1}, \tag{16c}$$

$$\dot{\eta}(t) = \min\{0, \sigma_{\mathrm{nom}}(t)\}, \quad \text{if } \|e(t)\| > e_{\min} \text{ and } \eta(t) = \sqrt{\eta_{\max} - \delta_3}, \tag{16d}$$

$$\dot{\eta}(t) = 0, \quad \text{otherwise}, \tag{16e}$$

for all $t \geq t_0$, where $\eta(t_0) \in \left[\sqrt{\delta_1}, \sqrt{\eta_{\max} - \delta_3}\right]$, and the initial conditions for each differential equation in (16) are chosen to enforce continuity of $\eta(\cdot)$ across switchings.

The roles of δ_1, δ_2, and δ_3 in (16) can be explained as follows. The user-defined parameter $\delta_1 > 0$ is to be set sufficiently small to enforce $\eta^2(t) \geq \delta_1$ for all $t \geq t_0$, since $\eta(\cdot)$ appears in the denominator of (13). The user-defined parameter δ_3 captures a lower bound on the diameter of the funnel for all $t \in [t_0, \infty)$. The tunable parameter δ_2 allows the user to impose a minimum distance between the funnel and the norm of the trajectory tracking error. This ensures that if an unexpected perturbation affects the plant and causes a sudden increase in the trajectory tracking error, the controller does not react with an excessive input in an attempt to enforce overly tight constraints, but relaxes the constraints on the tracking error until the diameter of the constraint set is $\eta_{\max} - \delta_1$; this feature is one of the key elements of the proposed control system since existing MRAC laws in the presence of constraints on the tracking error do not allow accommodating unmatched uncertainties by relaxing constraints within user-defined levels of tolerance. The threshold $e_{\min}$ given by (11) sets when to stop contracting the funnel. Indeed, if $\|e(t)\| \leq e_{\min}$, then $\eta(\cdot)$ is kept constant. The problem of setting $e_{\min} = \delta_3 = 0$ is left for future research. For a graphical representation of $\eta(\cdot)$ and the roles of $e_{\min}$, δ_1, δ_2, and δ_3, see Figure 2.

It follows from (12) and (16) that, in nominal conditions, that is, if the constraint set is free to contract at a user-defined rate, then

$$\dot{\eta}(t) = \eta(t)\xi(t), \quad \eta(t_0) = \eta_0, \quad t \geq t_0. \tag{17}$$

To account for saturation constraints on the plant actuators, we set

$$\xi(t) = \frac{u_{\max} - \|u(t)\|}{\max\{\|u(t)\| - u_{\min}, \Delta u_{\min}\}}, \quad t \geq t_0, \tag{18}$$

where $u_{\max} > u_{\min} \geq 0$ are user-defined and capture values related to the upper and lower saturation limits of the control input, respectively, and $\Delta u_{\min} > 0$ is user-defined. For additional details on this choice of $\xi(\cdot)$, see [5].

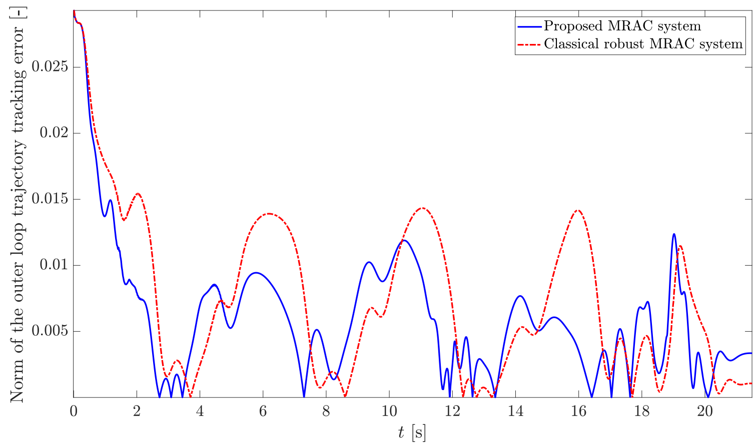

(a) Nominal conditions

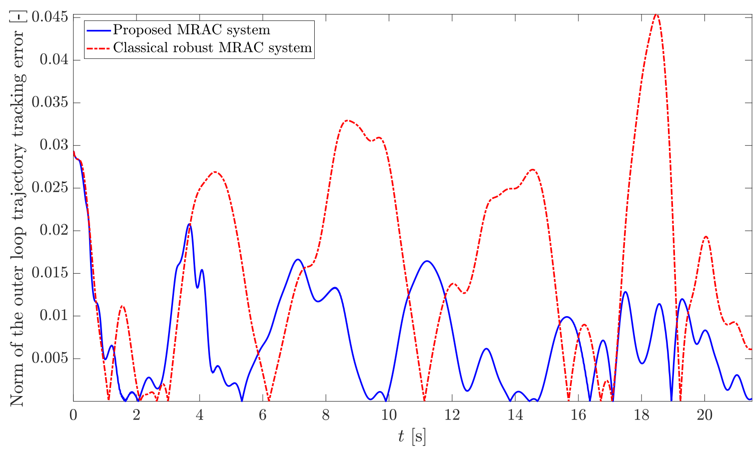

(b) Off-nominal conditions

Fig. 4 Norm of the trajectory tracking error for the translational dynamics in nominal and off-nominal conditions. Both in nominal and in off-nominal conditions, the proposed control system provides smaller tracking errors than its classical counterpart

Remark IV.1 *The constraints captured by* (9) *are* hard, *that is, inviolable constraints enforced by the control system at all times. The constraints enforceable through* $\xi(\cdot)$ *in* (16)*, such as, for instance,* (18) *are* soft, *that is, the proposed control system will attempt to enforce these constraints, which may be violated.*

The proposed MRAC system relies on the *control law*

$$\phi(\pi, \hat{K}) \triangleq \hat{K}^{\mathrm{T}}\pi, \quad (\pi, \hat{K}) \in \mathbb{R}^{n+m+N} \times \mathbb{R}^{(n+m+N)\times m}, \tag{19}$$

where $\pi(t) \triangleq \left[x^{\mathrm{T}}(t), r^{\mathrm{T}}(t), -\Phi^{\mathrm{T}}(t, x(t))\right]^{\mathrm{T}}$ and the *adaptive gain* $\hat{K} : [t_0, \infty) \to \mathbb{R}^{(n+m+N)\times m}$ verifies the *adaptive law*

$$\dot{\hat{K}}(t) = \mathrm{Proj}\left(\hat{K}(t), -\Gamma\mu(\|e(t)\|)H^{-1}(t, e(t))\left[\pi(t)e^{\mathrm{T}}(t)\left(P + V_e(t, e(t))M\right)B\right]\right), \quad \hat{K}(t_0) = \hat{K}_0, \quad t \geq t_0, \tag{20}$$

the *adaptive rate matrix* $\Gamma \in \mathbb{R}^{(n+m+N)\times(n+m+N)}$ is user-defined, symmetric, and positive-definite and

$$\mu(\alpha) \triangleq \begin{cases} 0 & \text{if } \alpha < E_0, \\ \frac{\alpha - E_0}{E_1 - E_0} & \text{if } \alpha \in [E_0, E_1], \\ 1 & \text{if } \alpha > E_1, \end{cases} \tag{21}$$

for all $\alpha \in [0, \infty)$, $E_0 \in [0, E_1)$ and $E_1 \in (0, \infty)$.

The adaptive law (20) merges the continuous projection operator discussed in Section III, with a modification of the classical dead-zone modification of MRA [28]. As already discussed, the continuous projection operator prevents parameter drift and enforces user-defined constraints on the adaptive gains. The classical deadzone modification turns off the adaptive rate whenever the tracking error is sufficiently small. In addition to preventing parameter drift, this tool reduces the stress on the actuators whenever the tracking error is sufficiently small and, hence, the controller's objectives are met. The classical deadzone modification of MRAC, however, is discontinuous and, hence, may produce chattering in the control input. To prevent this effect, the step discontinuity is approximated by the ramp function (21), whose clamping points E_0 and E_1 are user-defined.

Theorem IV.1 *Consider the plant model* (1)*, the reference model* (2)*, the adaptive law* (20)*, and* (16)*. If $e(t_0) \in \mathring{\mathcal{E}}_{t_0}$ and $u(t) = \phi(\pi(t), \hat{K}(t))$, $t \geq t_0$, where $\phi(\cdot, \cdot)$ is given by* (19)*, then $e(t) \in \mathring{\mathcal{E}}_t$ for all $t \geq t_0$, both $t \mapsto \hat{K}(t)$ and $t \mapsto \eta(t)$ are uniformly bounded on $[t_0, \infty)$, and the nonlinear, time-varying dynamical system given by* (1) *and* (20) *is uniformly ultimately bounded.*

A detailed proof of Theorem IV.1 is presented in [29]. It is worthwhile noting that, if no constraint is enforced, that is, $\eta_{\max} = 1$, $\eta(t) \equiv 0$, and $M = 0_{n\times n}$, or equivalently, $H(t, e) \equiv 1$ for all $(t, e) \in [t_0, \infty) \times \mathbb{R}^n$, then the control system presented reduces to a robust adaptive control system based on the convex projection operator and the dead-zone modification of MRAC. In the following, we refer to this control system as the classical counterpart of Theorem IV.1.

V. Numerical Simulations

This section presents the results of two sets of numerical simulations conducted in the PyChrono-based simulation environment [9]. The scope of these simulations is to verify the applicability of the proposed robust MRAC system on an autonomous X8-copter UAV and compare its performance to its classical counterpart. Figure 1 shows both the simulated UAV and its physical counterpart. The inertial properties of the simulated UAV are derived from a detailed CAD (computer-aided design) model of the actual vehicle. The X8 configuration has been chosen for its compact form factor, high thrust-to-volume ratio relative to non-coaxial multirotor platforms of comparable size or thrust, and the redundancy provided by the coaxial propulsion units. The mass of the UAV is 2.025 kg.

The first set of simulations, referred to as the *nominal conditions cases*, evaluates both the proposed controller and its classical counterpart in the absence of external disturbances and without a suspended payload. The second set of simulations, referred to as the *off-nominal conditions cases*, examines the controllers' performances when the UAV transports an unknown sling payload. This payload consists of a 0.530 kg steel ball with a diameter of 0.0508 m, attached to the UAV by a flexible rope whose connection geometry matches that of the physical platform shown in Figure 1. The payload's center of mass is located 0.140 m below the rope attachment point on the UAV. Notably, the payload mass corresponds to approximately 26% of the UAV's mass. In the simulation environment, the rope is modeled employing the `FEA` module of PyChrono. Hence, the flexibility of the rope is explicitly considered. Neither the flexible rope nor the payload is accounted for in the control system, which is discussed in detail in [5, 30], so that the payload is considered a mere disturbance.

In both sets of simulations, the same controller gains are used to emphasize each controller's ability to cope with the uncertainties introduced by the unknown payload. Furthermore, in both simulations, the UAV must track a minimum-jerk trajectory defined as a piecewise 7th-order polynomial interpolating 18 user-defined waypoints over a 21.5 s horizon, with a maximum velocity of 2.58 m/s and a peak acceleration of 5.45 $\mathrm{m/s^2}$. These waypoints have been obtained by sampling a three-dimensional lemniscate path; for details, see Figure 3. Throughout the mission, the desired UAV orientation is such that the roll axis remains tangent to the user-defined trajectory. Together with the user-defined trajectory, this requirement challenges both lateral and vertical tracking performance.

A. Mission in Nominal Conditions

This section evaluates the performance of both the proposed controller and its classical counterpart in the absence of external disturbances. These nominal conditions highlight the fundamental tracking capabilities of each control system.

Figure 4a illustrates the translational trajectory tracking error obtained using both Theorem IV.1 and its classical counterpart with $H(t, e) = 1$ for all $(t, e) \in [t_0, \infty) \times \mathbb{R}^n$. The proposed approach yields a noticeably smaller tracking error throughout the mission.

The total thrust commands generated during the nominal mission are shown in Figure 5a. The proposed controller exhibits more pronounced thrust variations, reflecting its ability to react promptly to tracking errors. Importantly, these

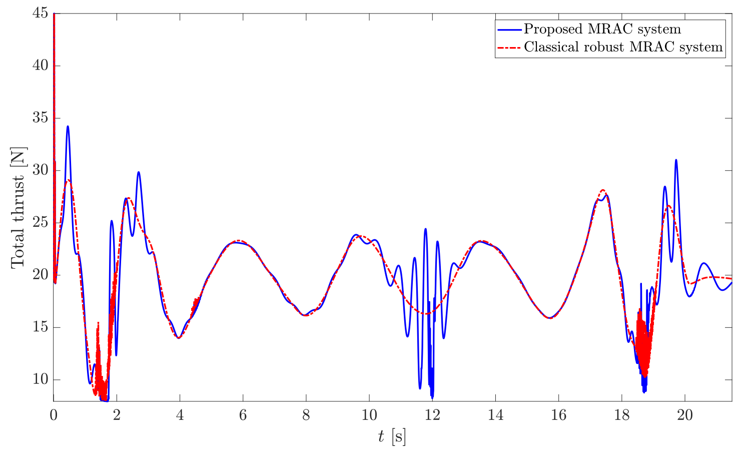

(a) Nominal conditions

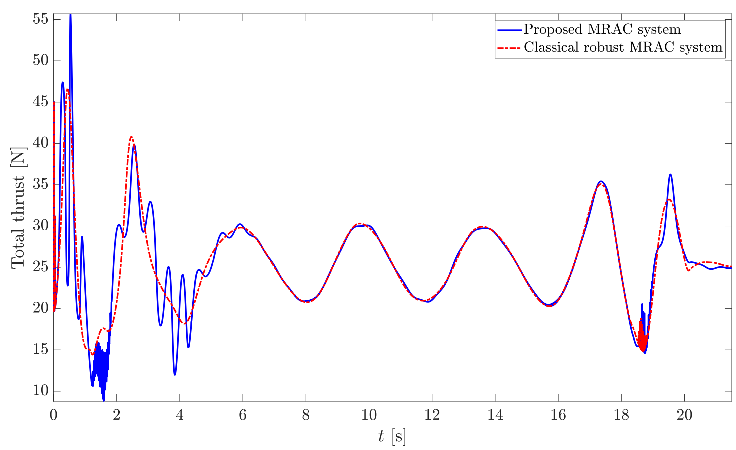

(b) Off-nominal conditions

Fig. 5 Total thrust required by the UAV in nominal and off-nominal conditions. Both in nominal and in off-nominal conditions, the two control systems require similar control inputs. However, the proposed control system requires a more aggressive policy to guarantee closer trajectory tracking. The thrust requested by each motor is within the saturation bounds allowed by the ESC-motor-propeller combination of the physical vehicle being simulated

variations remain within allowable bounds, confirming that the improved accuracy is obtained without compromising stability. Furthermore, the individual motor thrust profiles demonstrate that all commanded inputs remain feasible for both control algorithms, providing additional evidence that the robust adaptive funnel MRAC framework operates safely within actuator limits. Remarkably, the ESC-motor-propellers combination for the UAV shown in Figure 1 has been characterized experimentally as a function of the normalized control input provided by the flight control unit, a Pixhawk 6c. The spike in the thrust forces at $t = 0$ s is because, to accommodate the ball under the UAV in the off-nominal simulations, in both simulations, the UAV does not take off from the ground but at a distance of 0.02 m from the ground with zero initial velocity. Thus, both control systems produce a burst in thrust forces to overcome the initial free fall.

Overall, the nominal conditions mission demonstrates that the proposed controller achieves superior tracking performance. The proposed control system requires thrust forces that are compatible with those required by its classical counterpart.

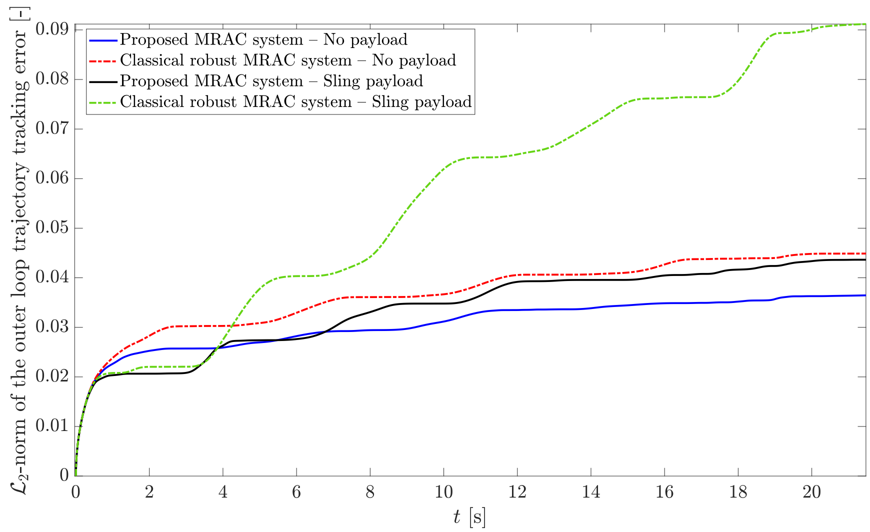

Fig. 6 $\mathcal{L}_2$-norm of the trajectory tracking error for the translational dynamics in nominal and off-nominal conditions. After the transient stage, in off-nominal conditions, the cumulative tracking error obtained applying the proposed control system is smaller than the cumulative tracking error obtained applying a classical robust MRAC system in nominal conditions

B. Mission in Off-Nominal Conditions

This section examines the performance of both controllers when the UAV is subject to off-nominal conditions induced by its sling payload. This scenario introduces significant unmodeled dynamics, representing a more challenging setting in which the robustness and adaptability of each controller can be meaningfully evaluated.

Figure 4b presents the translational trajectory tracking error for both control algorithms. The performance gap between the two controllers becomes significantly more pronounced than in the nominal case. The proposed robust adaptive funnel MRAC system yields a substantially lower tracking error throughout the mission, demonstrating its enhanced ability to cope with payload-induced uncertainties and sustain accurate tracking of the planned trajectory.

Executing the simulator available at [9], it is possible to appreciate the aggressiveness of the reference trajectory, which features rapid changes and coupled lateral and vertical motion. Despite the disturbances induced by the payload, the proposed MRAC system effectively tracks this demanding reference trajectory.

The total thrust commands generated during the off-nominal condition missions are shown in Figure 5b. Here, the similarities between the two controllers' efforts are more enhanced; however, the proposed controller still exhibits slightly larger oscillations due to its adaptive funnel mechanism and more responsive corrective behavior. Crucially, the thrust remains within acceptable limits throughout the maneuver.

Overall, the off-nominal conditions mission reinforces the advantages of the proposed robust adaptive funnel MRAC framework since it achieves markedly improved tracking accuracy relative to the robust classical MRAC system while maintaining feasible control inputs in the presence of substantial unmodeled dynamics.

Figure 6 presents the $\mathcal{L}_2$-norm of the translational trajectory tracking error for both controllers across both missions. The results clearly highlight the superior performance of the robust adaptive funnel MRAC framework. In off-nominal conditions, the proposed robust MRAC system achieves lower cumulative tracking error than its classical counterpart in nominal conditions.

Finally, Figure 7 shows both the evolution of the funnel diameter and the weighted norm of the tracking error over time for both missions. These plots illustrate the adaptive nature of the funnel mechanism, highlighting how it dynamically adjusts to maintain performance. The funnel diameter narrows when the actuators have enough bandwidth to do so, and expands when the actuators are reaching saturation or when the weighted norm of the tracking error is approaching the boundary of the funnel, enabling the controller to respond effectively under both nominal and off-nominal conditions.

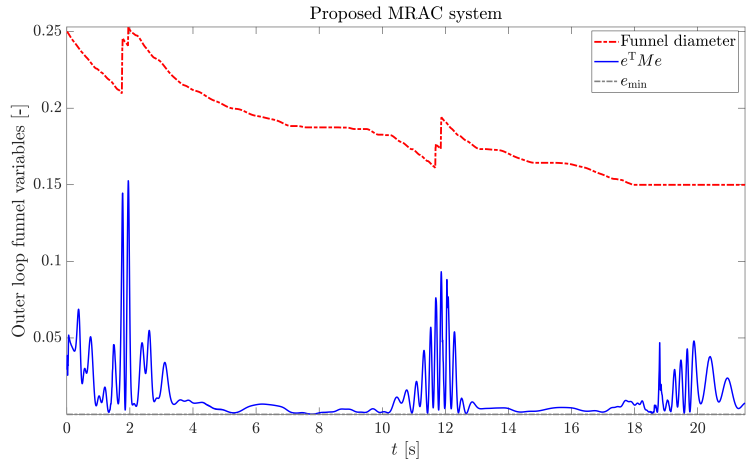

(a) Nominal conditions

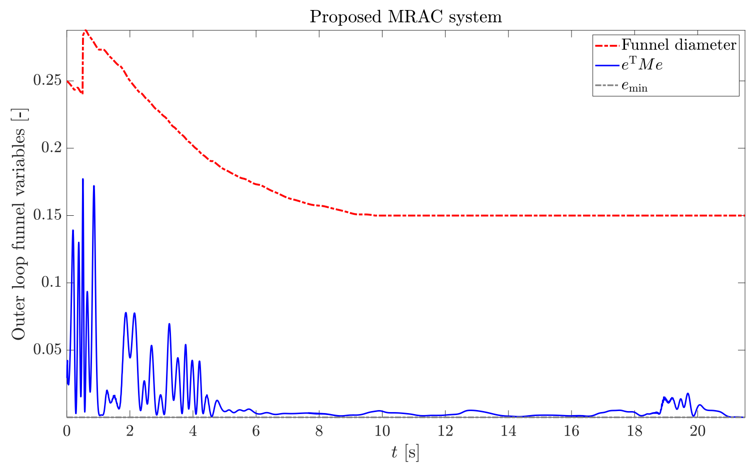

(b) Off-nominal conditions

Fig. 7 Funnel diameter and weighted norm of the trajectory tracking error in nominal and off-nominal conditions. Similarly to Figure 2, the diameter of the constraint set contracts over time to enforce increasingly smaller values of the tracking error

VI. Conclusion

This paper presented a robust MRAC system to enforce user-defined constraints on the trajectory tracking error. These constraints are a function of time, allowing both user-defined criteria on the rate of contraction of the constraint set and saturation of the system's actuators. A unique feature of this control system is that, within user-defined margins, the constraints on the trajectory tracking error can be relaxed to account for the effect of disturbances and modeling errors. This feature eases the applicability of the proposed results as it produces less aggressive control inputs than alternative adaptive control systems designed to enforce increasingly tighter constraints.

The effectiveness of the proposed theoretical results has been tested through high-fidelity numerical simulations by employing the proposed controller in the outer loop system of an X8 autonomous UAV. Two missions have been considered, namely a nominal mission, in which the UAV must follow a user-defined leminiscate trajectory, and an off-nominal mission, in which the UAV must follow the same trajectory while transporting a heavy ball connected to the vehicle by a flexible rope. In this off-nominal mission, the control system has not been re-tuned and is unaware of the presence of the payload. The performance of the proposed control system has been compared to that of its classical counterpart, that is, a robust MRAC system that does not enforce any constraints on the closed-loop plant model. Remarkably, in off-nominal conditions, the proposed MRAC system outperforms its classical counterpart in nominal conditions, while all tunable gains in common between the two controllers are kept identical.

Future work directions involve improvements of the proposed results to enforce arbitrarily small ultimate bounds on the trajectory tracking error. Furthermore, the proposed results will be tested experimentally on an X8-copter UAV.

Acknowledgments

This research was in part performed with the support of NSF through Grant no. 2137159 and the US Department of the Navy through Grant no. N004212520003.

The authors would like to express their gratitude to Mr. Giorgio A. Orlando for producing the initial version of the simulator employed in this paper and contributing to the literature review on control systems for UAVs transporting payloads connected by flexible ropes.

References

[1] Arabi, E., Gruenwald, B. C., Yucelen, T., and Nguyen, N. T., "A set-theoretic model reference adaptive control architecture for disturbance rejection and uncertainty suppression with strict performance guarantees," *International Journal of Control*, Vol. 91, No. 5, 2018, pp. 1195–1208. https://doi.org/10.1080/00207179.2017.1312019.

[2] L'Afflitto, A., "Barrier Lyapunov Functions and Constrained Model Reference Adaptive Control," *IEEE Control Systems Letters*, Vol. 2, No. 3, 2018, pp. 441–446. https://doi.org/10.1109/LCSYS.2018.2842148.

[3] Anderson, R. B., Marshall, J. A., and L'Afflitto, A., "Novel model reference adaptive control laws for improved transient dynamics and guaranteed saturation constraints," *Journal of the Franklin Institute*, Vol. 358, No. 12, 2021, pp. 6281–6308. https://doi.org/https://doi.org/10.1016/j.jfranklin.2021.06.020.

[4] Mirkin, B., Gutman, P.-O., and Shtessel, Y., "Tube reference model based direct adaptive control," *IFAC Proceedings Volumes*, Vol. 45, No. 13, 2012, pp. 553–558. https://doi.org/https://doi.org/10.3182/20120620-3-DK-2025.00092, 7th IFAC Symposium on Robust Control Design.

[5] Gramuglia, M., Kumar, G. M., and L'Afflitto, A., "Two-Layer Adaptive Funnel MRAC with Applications to the Control of Multi-Rotor UAVs," *2024 13th International Workshop on Robot Motion and Control (RoMoCo)*, 2024, pp. 31–36. https://doi.org/10.1109/RoMoCo60539.2024.10604361.

[6] Kurdila, A. J., L'Afflitto, A., and Burns, J. A., *Data-Driven, Nonparametric, Adaptive Control Theory*, Springer, London, UK, 2025. https://doi.org/10.1007/978-3-031-78003-5.

[7] Tasora, A., Serban, R., Mazhar, H., Pazouki, A., Melanz, D., Fleischmann, J., Taylor, M., Sugiyama, H., and Negrut, D., "Chrono: An open source multi-physics dynamics engine," *High Performance Computing in Science and Engineering – Lecture Notes in Computer Science*, edited by T. Kozubek, Springer, 2016, pp. 19–49.

[8] Project Chrono, "Chrono: An Open Source Framework for the Physics-Based Simulation of Dynamic Systems," https://projectchrono.org/, 2014. Accessed: 2025-11-14.

[9] Gramuglia, M., Kumar, G. M., and L'Afflitto, A., "A PyChrono-Based High-Fidelity Simulator for UAVs," https://github.com/andrealaffly/UAV_Sim_PyChrono, 2025. Version 1.0.0, accessed 2025-11-19.

[10] Sreenath, K., Lee, T., and Kumar, V., "Geometric control and differential flatness of a quadrotor UAV with a cable-suspended load," *IEEE Conference on Decision and Control*, 2013, pp. 2269–2274. https://doi.org/10.1109/CDC.2013.6760219.

[11] Tang, S., and Kumar, V., "Mixed Integer Quadratic Program trajectory generation for a quadrotor with a cable-suspended payload," *International Conference on Robotics and Automation*, 2015, pp. 2216–2222. https://doi.org/10.1109/ICRA.2015.7139492.

[12] Yu, G., Cabecinhas, D., Cunha, R., and Silvestre, C., "Aggressive maneuvers for a quadrotor-slung-load system through fast trajectory generation and tracking," *Autonomous Robots*, Vol. 46, No. 4, 2022, pp. 499–513. https://doi.org/10.1007/s10514-022-10035-y.

[13] Yang, S., Xian, B., Cai, J., and Wang, G., "Finite-Time Convergence Control for a Quadrotor Unmanned Aerial Vehicle With a Slung Load," *IEEE Transactions on Industrial Informatics*, Vol. 20, No. 1, 2024, pp. 605–614. https://doi.org/10.1109/TII.2023.3268762.

[14] Kang, J., Shan, J., and Alkomy, H., "Control Framework for a UAV Slung-Payload Transportation System," *IEEE Control Systems Letters*, Vol. 7, 2023, pp. 2473–2478. https://doi.org/10.1109/LCSYS.2023.3285421.

[15] Arizaga, J. M., Miranda-Moya, A., Castañeda, H., and Castillo, P., "Observer-based adaptive control for slung payload stabilization with a fully-actuated multirotor UAV," *ISA Transactions*, Vol. 147, 2024, pp. 109–117. https://doi.org/https://doi.org/10.1016/j.isatra.2024.02.015.

[16] Yang, S., and Xian, B., "Energy-Based Nonlinear Adaptive Control Design for the Quadrotor UAV System With a Suspended Payload," *IEEE Transactions on Industrial Electronics*, Vol. 67, No. 3, 2020, pp. 2054–2064. https://doi.org/10.1109/TIE.2019.2902834.

[17] Yu, G., Reis, J., Cabecinhas, D., Cunha, R., and Silvestre, C., "Reduced-Complexity Active Disturbance Rejection Controller for Quadrotor-Slung-Load Transportation," *IEEE Transactions on Systems, Man, and Cybernetics: Systems*, Vol. 53, No. 8, 2023, pp. 5248–5259. https://doi.org/10.1109/TSMC.2023.3263881.

[18] Wang, S., Chen, H., Liu, J., and Liu, Y., "Adaptive trajectory tracking of UAV with a cable-suspended load using vision-inertial-based estimation," *Automatica*, Vol. 158, 2023, p. 111310. https://doi.org/https://doi.org/10.1016/j.automatica.2023.111310.

[19] Salinas, L. R., Gimenez, J., Gandolfo, D. C., Rosales, C. D., and Carelli, R., "Unified Motion Control for Multilift Unmanned Rotorcraft Systems in Forward Flight," *IEEE Transactions on Control Systems Technology*, Vol. 31, No. 4, 2023, pp. 1607–1621. https://doi.org/10.1109/TCST.2023.3240541.

[20] Yu, G., Cabecinhas, D., Cunha, R., and Silvestre, C., "Nonlinear Backstepping Control of a Quadrotor-Slung Load System," *IEEE/ASME Transactions on Mechatronics*, Vol. 24, No. 5, 2019, pp. 2304–2315. https://doi.org/10.1109/TMECH.2019.2930211.

[21] Lv, Z., Wu, Y., Sun, X.-M., and Wang, Q.-G., "Fixed-Time Control for a Quadrotor With a Cable-Suspended Load," *IEEE Transactions on Intelligent Transportation Systems*, Vol. 23, No. 11, 2022, pp. 21932–21943. https://doi.org/10.1109/TITS.2022.3180733.

[22] Qian, L., and Liu, H. H., "Path-Following Control of A Quadrotor UAV With A Cable-Suspended Payload Under Wind Disturbances," *IEEE Transactions on Industrial Electronics*, Vol. 67, No. 3, 2020, pp. 2021–2029. https://doi.org/10.1109/TIE.2019.2905811.

[23] Wu, Y., Xie, Y., and Li, S., "Parameter Adaptive Control for a Quadrotor With a Suspended Unknown Payload Under External Disturbance," *IEEE Access*, Vol. 9, 2021, pp. 139958–139967. https://doi.org/10.1109/ACCESS.2021.3119396.

[24] Bernard, M., and Kondak, K., "Generic slung load transportation system using small size helicopters," *International Conference on Robotics and Automation*, IEEE, Kobe, Japan, 2009, pp. 3258–3264. https://doi.org/10.1109/ROBOT.2009.5152382.

[25] Dai, S., Lee, T., and Bernstein, D. S., "Adaptive control of a quadrotor UAV transporting a cable-suspended load with unknown mass," *IEEE Conference on Decision and Control*, Los Angeles, LA, 2014, pp. 6149–6154. https://doi.org/10.1109/CDC.2014.7040352.

[26] Ioannou, P., and Fidan, B., *Adaptive Control Tutorial*, Society for Industrial and Applied Mathematics, Philadelphia, PA, 2006.

[27] Lavretsky, E., and Wise, K., *Robust and Adaptive Control: With Aerospace Applications*, 2^{nd} ed., Springer, London, UK, 2024.

[28] Peterson, B., and Narendra, K., "Bounded error adaptive control," *IEEE Transactions on Automatic Control*, Vol. 27, No. 6, 1982, pp. 1161–1168. https://doi.org/10.1109/TAC.1982.1103112.

[29] Gramuglia, M., Kumar, G. M., and L'Afflitto, A., "Robust Two-Layer MRAC to Enforce Competing Constraints," *IEEE Transactions on Automation Science and Engineering*, 2025. In review.

[30] Gramuglia, M., Kumar, G. M., and L'Afflitto, A., "A Hybrid Model Reference Adaptive Control System for Multi-Rotor Unmanned Aerial Vehicles," *SciTech*, AIAA, Orlando, FL, 2024, pp. 1–21. https://doi.org/10.2514/6.2024-0755.